Interaction between OH Radical and the Water Interface

Shiyu Du and Joseph S. Francisco*

Department of Chemistry and Department of Earth and Atmospheric Sciences, Purdue University, West Lafayette, Indiana 47907-1393

Received: October 31, 2007; Revised Manuscript Received: March 10, 2008

Results from a theoretical study of the interactions of a OH radical on $(H_2O)_{20}$, $(H_2O)_{24}$, and $(H_2O)_{28}$ clusters used as a novel model of a water droplet are presented. This work shows that there is competition between OH radicals trapped on the surface and those encapsulated inside of a water cage. This is contrary to previous findings of HO_2 radical interactions with water clusters. Natural bond orbital (NBO) analysis is used to analyze the bonding feature of OH to help explain the difference in behavior between OH and HO_2 radicals toward a water surface.

I. Introduction

The behavior of free radical−molecule complexes are of interest to the study of atmospheric chemistry because radical reactions in the atmosphere can be affected by the uptake of radicals by aqueous aerosols and cloud droplets. One of the most important and reactive species is the hydroxyl radical (OH). It is a key oxidant in the lower atmosphere as it initiates oxidation of most trace species including volatile organic compounds (VOCs).[1,2] Due to the significance of hydroxyl radical chemistry in the atmosphere, a number of studies have focused on the in situ measurements of OH radicals. Previous theoretical and experimental studies of OH gas-phase reactions in the atmosphere also focused on reactions in the remote, cloud-free troposphere.[3–5] Measurement of OH abundances in and around clouds has been performed by Mauldin et al.[5] The calculation of OH abundances showed good agreement with the experimental results from the selected ion chemical ionization mass spectrometry (SICIMS) in the cloud-free areas but overpredicted the OH concentrations when passing through the cloud.

There are several forms of water in the cloudy atmosphere including gaseous water clusters, cloud droplets, and liquid aerosols. Hydrogen-bonding interaction between free radicals and water molecules play an important role in controlling the abundance and chemical behavior of free radicals in the atmosphere. An investigation into the binding patterns in which radicals are incorporated into clouds and aerosols is crucial to the understanding of their atmospheric behavior.[6] Moreover, it is essential to understand the reactive uptake processes in the atmosphere involving radicals. The motivation of this paper is to provide a new insight into the above perspectives of free radicals in the atmosphere by studying characteristics of the interactions between an OH radical and large water clusters.

In previous work, using molecular dynamics (MD) simulations, Roeselova et al.[7] explored the dynamics of the molecular interactions between OH and a bulk liquid water interface. They found that the OH radical spent a greater time outside of the water slab than inside. The same group, in a later study, provided molecular-level insight into the process, revealing that a gas-phase hydroxyl radical with thermal impact velocity becomes accommodated at the water surface and/or is taken up into the bulk liquid.[8] Couto et al.[9] studied hydration of the OH radical with Monte Carlo simulations. The protonated water clusters with cage structures are reported in some recent experimental work.[10,11] The MD simulation methods are limited by the accuracy of force fields and cannot provide as accurate of a prediction on the stationary points on the potential energy surface (PES) as can ab initio calculations. Stationary points of the complex can give a clear view of the most stable configurations when the OH radical is binding with or being incorporated into a water droplet. Moreover, the MD simulations cannot give any insight into the bonding features between a OH radical and the surface of water molecules in clouds, which is integral to the understanding of OH's accommodation into water droplets in the atmosphere. The bonding can only be studied meaningfully on stationary points of an ab initio potential energy surface.

Another approach to evaluate the effect that water molecules have on free radicals in the atmosphere is to study the interaction between free radicals and water clusters through electronic structure calculations.[6,12–15] Shi, Belair, and Francisco et al.[6] used a cage structure $(H_2O)_{20}$ molecular cluster to model a small water droplet in the atmosphere in order to investigate the interaction between the HO_2 radical and atmospheric aerosols. Their molecular cluster has a four-layer spherical cage structure formed by hydrogen-bonded water molecules. Their calculations predicted three types of minima on the PES, of which the structure with HO_2 bound to the top of the water cluster is the global minimum. With the same model, Belair et al.[16] employed natural bond orbital (NBO) theory[17–21] to gain further insight into the bonding between the HO_2 radical and a water droplet surface. It was found that interactions between the radical and the water surface are localized. In the present work, a study of the interaction between a OH radical and a similar cage structure of a water cluster, $(H_2O)_{20}$, is performed using ab initio methods. In addition, larger cage structures are employed to explore whether interactions similar to those found in the $(H_2O)_{20}$ cage are involved. Up to now, no quantum chemical study has been performed looking at the interaction between OH and large water clusters. The interaction between the OH radical and a water droplet is presented in detail here in order to understand how this radical behaves in the atmosphere in the presence of cloud droplets. In order to study the interaction between the OH radical and water clusters of larger sizes with reasonable computational

* To whom correspondence should be addressed.

10.1021/jp710509h CCC: $40.75
Published on Web 05/03/2008

cost, calculations utilize the recently developed empirical potential.[22–26]

II. Method and Computational Details

Although there are many hydrogen-bonding isomers for the $(H_2O)_{20}$ cluster,[27–31] in this work, a cage structure of the $(H_2O)_{20}$ cluster is used as the model of a water droplet. Because the binding energy of $(H_2O)_{20}\cdot OH$ will be overpredicted if the totally symmetric cage structure is used, as shown in the literature,[6] a new deformed $(H_2O)_{20}$ cage structure is chosen as the reference in the present work. Full geometry optimizations on the potential energy surface of the $(H_2O)_{20}\cdot OH$ system are performed with two levels of theories, unrestricted Hartree−Fock (UHF)[20] and unrestricted Becke's three-parameter density functional with the Lee, Yang, and Parr functional to describe gradient-corrected correlation effects (UB3LYP)[32] with a 6-31G(d) basis set. Since the interaction between a HO_2 radical and a $(H_2O)_{20}$ cluster has been well studied at the level of UHF/6-31G(d),[6,16] the behavior of a OH radical interacting with a water droplet can be qualitatively described by the calculations at the same level of theory. Three different types of minima were found for the approach of the OH radical to the surface of the $(H_2O)_{20}$ cluster, and all were confirmed via frequency analysis. Single-point energy calculations on the optimized structures were performed using second-order Moller−Plesset perturbation theory (MP2)[33–35] in order to determine the binding energy (B.E.). The B.E. is calculated via the equation

$$\text{B.E.} = \text{E}[(H_2O)_{20}\cdot OH] - \text{E}[(H_2O)_{20}] - \text{E[OH]}, \quad (1)$$

where $E[(H_2O)_{20}\cdot OH]$, $E[(H_2O)_{20}]$, and E[OH] are energies of the $(H_2O)_{20}\cdot OH$ complex, $(H_2O)_{20}$ at the optimized geometry, and OH at the optimized geometry, respectively. Similarly, the binding energies of OH complexes with larger water clusters of size n (n = 24, 28) are calculated by the difference of empirical potential

$$\text{B.E.} = E[(H_2O)_n\cdot OH] - E[(H_2O)_n] \quad (2)$$

In order to evaluate the change in stability of the water cluster, the relaxation energy (RX.E.) of the water cluster is also calculated as follows

$$\text{RX.E.} = E^{C}[(H_2O)_{20}] - E^{O}[(H_2O)_{20}] \quad (3)$$

where $E^{C}[(H_2O)_{20}]$ and $E^{O}[(H_2O)_{20}]$ are energies of $(H_2O)_{20}$ at the complex geometry and at the optimized geometry, respectively.

The potential energy surfaces (PES) are scanned in order to understand how the free radical approaches the water droplet surface. Every point on the PES is optimized at the UHF/6-31G(d) level of theory with geometry constraints. The calculations are performed with the Gaussian98,[36] Gaussian03,[37] and NWCHEM[38] at EMSL in the Pacific Northwestern National Laboratory (PNNL).[39] The NBO[17] analysis is carried out using the NBO 5.0[40] software packages.

III. Results and Discussions

A. OH Radical Interaction with a Water Surface. Starting with the four-layer totally symmetric dodecahedral water molecule cluster (cage structure) reported in the literature[6] and shown in Figure 1 to model a water droplet, the present work shows that the binding energies will be overpredicted when using this symmetric cage structure water cluster as the reference for the $(H_2O)_{20}\cdot OH$ system. With such a reference structure, the stability of the $(H_2O)_{20}\cdot OH$ complexes is partly due to the rearrangement of the water cluster instead of the bonding

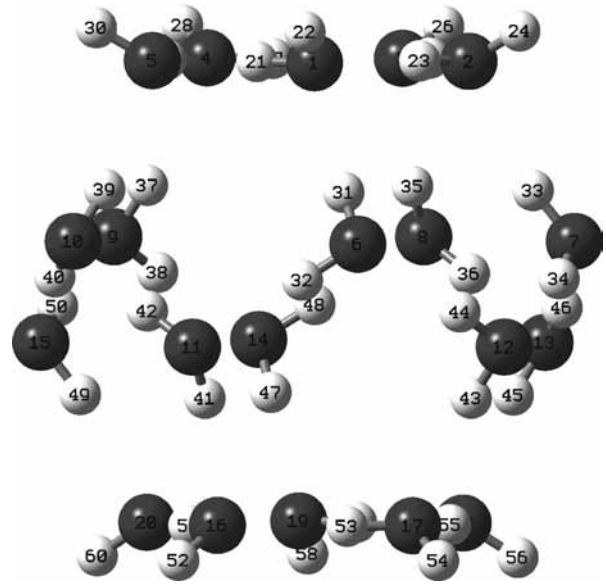

Figure 1. $(H_2O)_{20}$ totally symmetric structure.

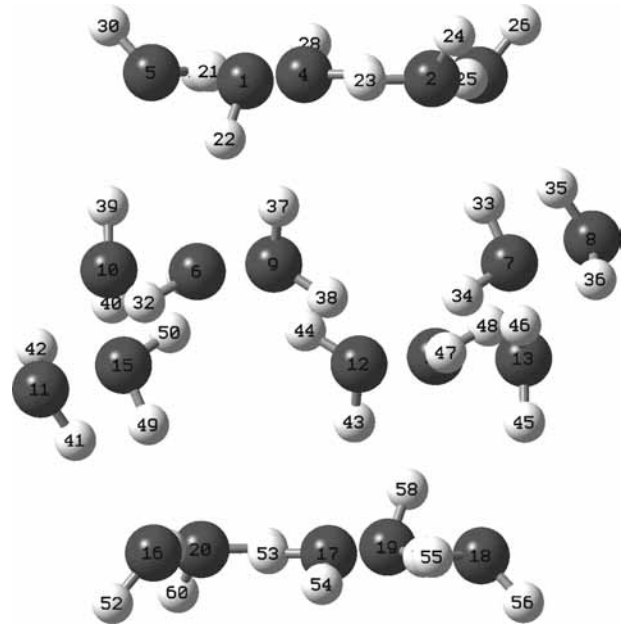

Figure 2. Symmetry-relaxed $(H_2O)_{20}$ structure.

interaction between the water molecules and the OH radical. To accurately predict the binding energy, a symmetry-relaxed four-layer $(H_2O)_{20}$ cage structure is used (Figure 2). The numbering system is the same as that for the symmetric cage structure,[6] in which the 20 water molecules are divided into four layers (L1−L4). In each layer, there are five water molecules. The 20 water molecules are numbered from W_1 to W_{20}, their oxygen atoms are labeled from O_1 to O_{20}, and their hydrogen atoms are from H_{21} to H_{60}. In the symmetric structure, the top and bottom layers are both composed of cyclic pentamer rings, in which each water molecule has one hydrogen atom dangling and the other hydrogen bonded. In the symmetry-relaxed structure (Figure 2), four of the five water molecules behave similar to those in the symmetric structure, and the two hydrogen atoms in the fifth molecule are engaged in hydrogen bonding. As shown in Figure 2, the hydrogen atoms on water No. 1 (W_1) and water No. 19 (W_{19}) formed hydrogen bonds with the water molecule in the layer between them. This caused water No. 8 (W_8) and water No. 1 (W_{11}) to protrude from their

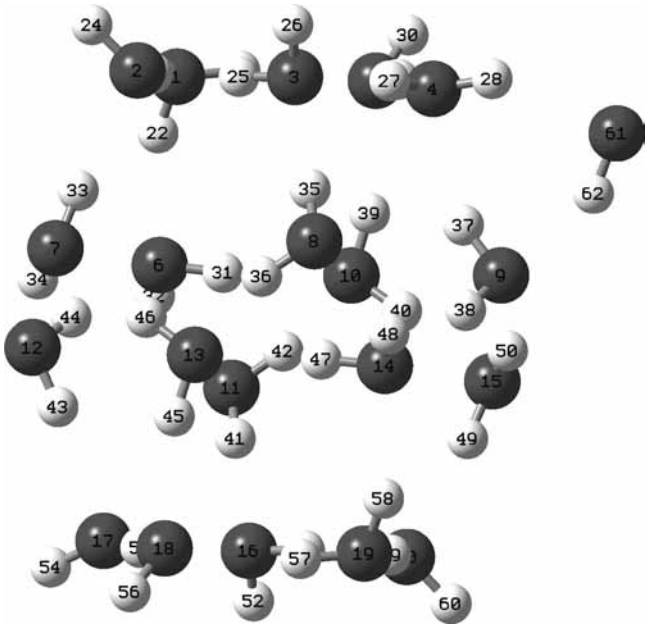

Figure 3. $[(H_2O)_{20}\cdot OH]^{OUT,SIDE}$ structure.

positions in the symmetric structure. As a result, this deformed structure has 32 hydrogen atoms which participate in hydrogen bonds and 8 dangling, compared with 30 participating in hydrogen bonds and 10 dangling in the totally symmetric structure. This structure was optimized at both the B3LYP/6-31G(d) and HF/6-31G(d) levels of theory. Single-point energy calculations show that the resulting structure is about 10 kcal/mol more stable than the symmetric structure at the level of HF/6-31G(d) and 16 kcal/mol more stable at the level of MP2/6-31G(d)//HF/6-31G(d). The average binding energy per hydrogen bond is predicted to be 6.1 kcal/mol, very close to 6.2 kcal/mol,[6] for the totally symmetric structure. This suggests that the stability for hydrogen bonding brought by the cage structure is still in the symmetry-relaxed structure.

Because of the existence of multiple potential binding sites on the water cluster for the OH radical, there may be a large number of minima in the potential energy surface of the $(H_2O)_{20}\cdot OH$ system. In this work, the minima that maintain the spherical structure of the water cluster are examined, and three different types of optimized isomers of $(H_2O)_{20}\cdot OH$ complexes are found. They are $[(H_2O)_{20}\cdot OH]^{OUT,SIDE}$, $[(H_2O)_{20}\cdot OH]^{OUT,TOP}$, and $[(H_2O)_{20}\cdot OH]^{IN}$, shown in Figures 3, 5, and 7, respectively. The oxygen and hydrogen atoms in the OH radical are labeled O_{61} and H_{62}. The OH radical forms two different hydrogen bonds with the water cluster, in one of which OH is acting as a hydrogen acceptor and in the other of which OH is acting as a hydrogen donor. Their relative energies are listed in Table 1 after correction for the basis set superposition error (BSSE)[41] in each calculation. The relaxation energies are all found to be positive, indicating that the molecular cluster is partially destabilized when a free radical is bound to the water droplet; therefore, the stability of the complexes are all from the hydrogen bonding between water molecules and the free radical. In fact, the relaxation energies will all be negative if the symmetric structure is used as the reference at both levels of theory. This validates the use of the symmetry-relaxed cage structure.

For the configuration of $[(H_2O)_{20}\cdot OH]^{OUT,SIDE}$ as shown in Figure 3, the oxygen atom in the free radical (O_{61}) is bound to H_{28} in L1, and the hydrogen atom (H_{62}) is bound to O_9 in L2. The formation of these hydrogen bonds appears to bend both

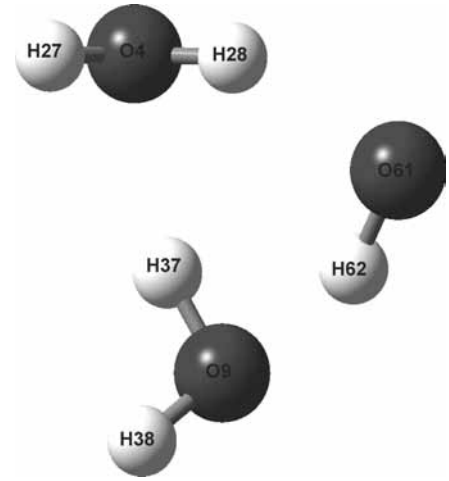

Figure 4. The three-molecule structure from the $[(H_2O)_{20}\cdot OH]^{OUT,SIDE}$ complex.

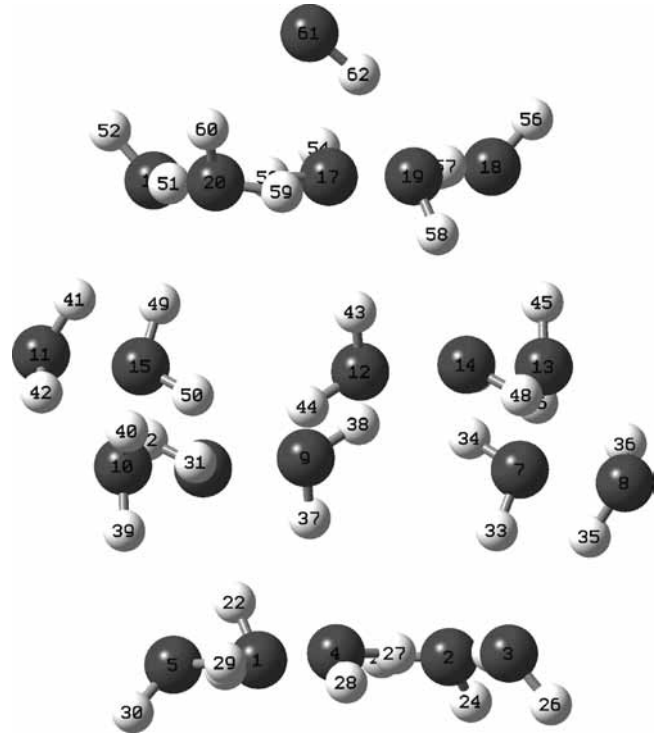

Figure 5. $[(H_2O)_{20}\cdot OH]^{OUT,TOP}$ structure.

the O−H bonds of W_4 and W_9; however, the overall configuration of the water cluster is kept. The binding energy of this structure is 9.3 kcal/mol after BSSE correction at the MP2/6-31G(d)//B3LYP/6-31G(d) level. From the relaxation energy and the $[(H_2O)_{20}\cdot OH]^{OUT,SIDE}$ configuration, we can see that the stability of the water cluster in this structure is the least affected of the three structures by the introduction of the hydrogen bond by the free radical. The configuration of the two water molecules hydrogen bound to a OH radical is shown in Figure 4. This relative orientation is consistent with that in the fully optimized $(H_2O)_2\cdot OH$ structure.[9] If isolated from the complex, the interaction energy between OH and $(H_2O)_2$ in the three-molecule structure at the complex geometry is 10.1 kcal/mol at the level of UMP2/6-31G(d)//UB3LYP/6-31G(d) after BSSE correction. This is only 0.8 kcal/mol more than that of the optimized $(H_2O)_{20}\cdot OH$ complex. This result seems to suggest that the stability energy of the three-molecule structure in the complex is localized. However, we cannot conclude that the interaction

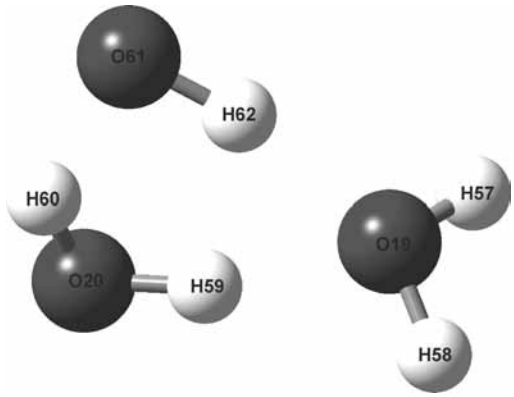

Figure 6. The three-molecule structure from the $[(H_2O)_{20}\cdot OH]^{OUT,TOP}$complex.

TABLE 1: The Binding Energies (B.E.) of the Complexes and Relaxation Energies (RX.E.) of the Corresponding Water Clusters; All Calculations Performed with the Basis Set 6-31G(d)

	RX.E. of $(H_2O)_{20}$ MP2//HF (kcal/mol)	RX.E. of $(H_2O)_{20}$ MP2//B3LYP (kcal/mol)	B.E. MP2// B3LYP[a] (kcal/mol)
SIDE	0.02	0.90	−9.3
TOP	0.96	1.91	−6.4
IN	1.32	1.44	−9.8

[a] BSSE-corrected energies.

is unaffected by other water molecules. To understand the orbital change in the presence of other water molecules, a NBO analysis is used to evaluate this effect. A detailed NBO analysis is presented and discussed in section B.

As to the $[(H_2O)20\cdot OH]^{OUT,TOP}$ configuration in Figure 5, the O_{61} atom forms a hydrogen bond with the H atom (H_{60}) in W_{20}, and the H_{62} atom is hydrogen bound to the oxygen (O_{19}) in W_{19}, which does not have a dangling H atom in L1(4). The complexation between the two moieties occurs only in the first layer of the water cluster. The BSSE-corrected binding energy of this structure is 6.4 kcal/mol at the level of MP2/6-31G(d)// B3LYP/6-31G(d), which is smaller than that calculated for $[(H_2O)_{20}\cdot OH]^{OUT,SIDE}$. The distortion of the water cluster occurs on W_{14}, W_{18}, and W_{20}, and an observable bending of their hydrogen bonds with W_{19} is found. The extracted three-molecule structure including W_{19}, W_{20}, and the free radical from the complex is shown in Figure 6. This arrangement of the three moieties is quite different from the fully optimized $(H_2O)_2\cdot OH$ structure. Both hydrogen atoms on W_{19} participate in hydrogen bonds, and W_{20} act as a double hydrogen donor. A single-point calculation on this isolated three-molecule structure shows a binding energy of only 1.8 kcal/mol between OH and $(H_2O)_2$, much less than that of $(H_2O)_{20}\cdot OH$. The large difference in binding energy of the whole complex and the three-molecule structure may be a reflection of the orbital orientation difference. As a result of the bending of the hydrogen bonds, the final relaxation energy of the water cluster in this structure is larger than that in $[(H_2O)_{20}\cdot OH]^{OUT,SIDE}$.

In the $[(H_2O)_{20}\cdot OH]^{IN}$ configuration (Figure 7), the OH radical is caged inside of the $(H_2O)_{20}$ cluster. To accommodate the OH radical, some of the O−H bonds of the water molecules have to bend toward the inside of the cluster, for exampls, the orientations of $O_{14}-H_{47}$, O_6-H_{31}, and $O_{12}-H_{47}$ all undergo observable changes. Because of the hydrogen bonding to the hydroxyl radical, W_{15} moves toward the inside. This movement results in alterations in the position and orientation of the water

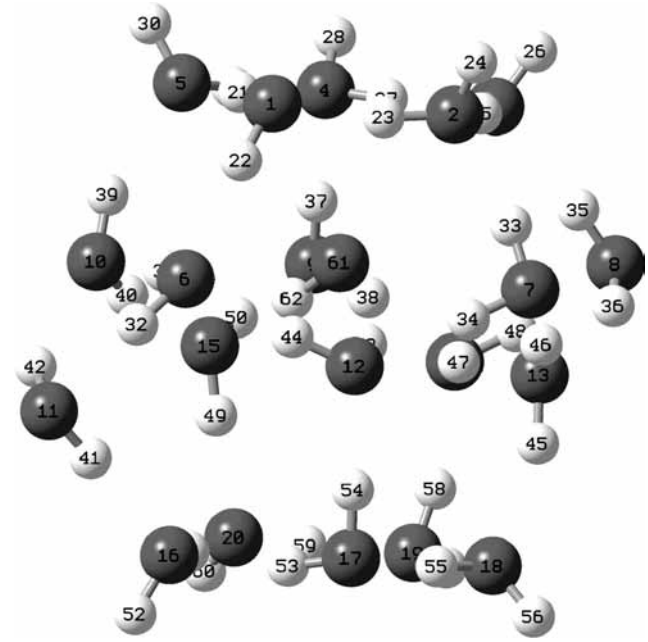

Figure 7. $[(H_2O)_{20}\cdot OH]^{IN}$ structure.

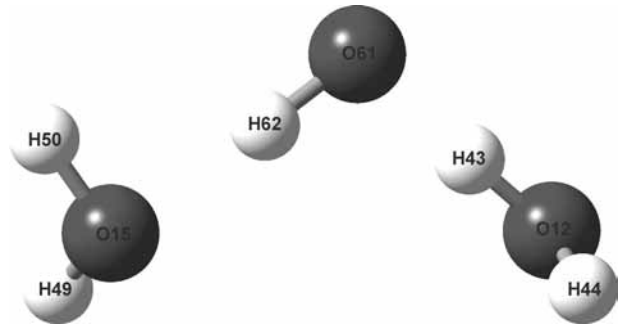

Figure 8. The three-molecule structure from the $[(H_2O)_{20}\cdot OH]^{IN}$ complex.

molecules surrounding W_{15}. The most distinct hydrogen bonds are those formed by the H atom on W_{12} with the O atom on the radical and by the O atom on W_{15} with the H atom on the radical. This is shown in Figure 8. Since there is a greater deal of structural rearrangement in this configuration than for the other two complexes, the interaction between the free radical and the water cluster is more likely a delocalized one. The MP2 single-point energy calculation shows that the binding energy of this structure is 9.8 kcal/mol after BSSE correction at the UMP2/6-31G(d)//B3LYP/6-31G(d) level of theory, which is about 0.5 kcal/mol lower than that for $[(H_2O)_{20}\cdot OH]^{OUT,SIDE}$. The small difference in binding energies may be due to a stronger delocalization effect in the $[(H_2O)_{20}\cdot OH]^{IN}$ structure. In order to assess the effect of basis sets on the relative stability of the three complexes, we made single-point calculations on the three optimized structures at the level of UMP2/6-311+G(d, p)//B3LYP/6-31G(d). The binding energies are 9.98, 8.97, and 15.56 kcal/mol for $[(H_2O)_{20}\cdot OH]^{OUT,SIDE}$, $[(H_2O)_{20}\cdot OH]^{OUT,TOP}$, and $[(H_2O)_{20}\cdot OH]^{IN}$, respectively, which shows a trend that is consistent with the results from the 6-31G(d) basis set. As a comparison, the binding energies for the three structures are calculated with our recently developed empirical potential[22] between a water molecule and the OH radical (mTTM model) and Xantheas' potential between water molecules (TTM2-R model),[23–26] which have been discussed in detail elsewhere.[22–26] We obtain 9.82, 9.02, and 16.86 kcal/mol for (OUT,SIDE), (OUT,TOP), and IN structures, respectively. These show an

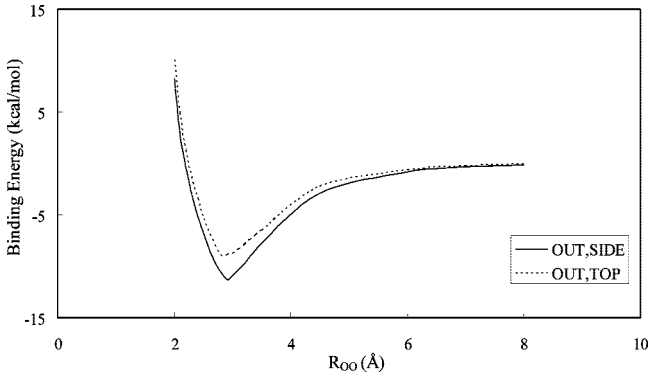

Figure 9. The potential energy surface scan of the $[(H_2O)_{20}\cdot OH]^{OUT,SIDE}$ and $[(H_2O)_{20}\cdot OH]^{OUT,TOP}$ structures at the level of HF/6-31G(d).

excellent agreement with our ab initio results at the highest level of theory. Since our empirical potential is constructed by fitting parameters to the ab initio PES at the level of an all-electron coupled cluster method involving single and double excitations with a perturbation estimation of the triple excitations[42–45] with the basis set of augmented correlation-consistent basis sets of triple-ζ quality,[46,47] that is, the RCCSD(T)/aug-cc-pVTZ level, the consistency is an indication of the qualitative reliability of the quantum chemical calculation results.

In order to understand how a free radical interacts with the water interface, the potential energy surface (PES) of the $[(H_2O)_{20}\cdot OH]^{OUT,SIDE}$ and $[(H_2O)_{20}\cdot OH]^{OUT,TOP}$ complexes are scanned. To accurately predict the energies and allow geometrical changes during the scans, partial optimizations of the PES are performed for the $[(H_2O)_{20} + \bullet OH]$ clusters with fixed distances between the oxygen atom of the free radical and the closest oxygen atom in the water molecular cluster, defined as R_{OO}. The scans are performed with optimization on every point on the PES of OH from both the "OUT, TOP" and "OUT, SIDE" directions toward the $(H_2O)_{20}$ cluster. When the distance is smaller than that in the fully optimized structure, one angle and one dihedral defined with most adjacent O atoms are also fixed to maintain the OH radical in the proper direction toward the $(H_2O)_{20}$ moiety. Using this method, information on how the free radical and the water droplet relax and how they affect each other when the two moieties approach each other can be examined. The distance scanned is from 8.0 to 2.0 Å at the level of HF/6-31G(d). The data are plotted in Figure 9. As seen in the figure, at large distances ($R_{OO} \sim 5.0-8.0$ Å), the energy of the system is very close to the sum of the water cluster and OH radical energies, indicating that the interaction between them is negligible, as expected. As R_{OO} decreases, the total system energy continues decreasing until R_{OO} is about 2.9 Å, which shows a net attraction between the water droplet and the OH radical. The above trend shows that the attraction causes their complexation, and the system reaches a stable configuration at the minimum point on the PES. The binding energy from the potential energy surface for the $[(H_2O)_{20}\cdot OH]^{OUT,SIDE}$ configuration is larger than that of $[(H_2O)_{20}\cdot OH]^{OUT,TOP}$, which is consistent with the energy prediction discussed earlier. Calculations also show that both structures show the same distance ($R_{OO} = 2.9$ Å) at the minimum point on the PES. When R_{OO} is less than 2.5 Å, the interaction rapidly becomes increasingly repulsive with decreasing R_{OO}, as shown in the figure. This trend suggests that the formation of a complex with •OH inside of the water cluster requires the water molecules to undergo a major rearrangement in order to avoid the high energy barrier when the radical diffuses into a water surface. This means that the complex with OH inside of the water cluster is much less favorable kinetically. The kinetic effect is atmospherically important since water molecules on an aerosol surface interchange between liquid and gas phases several times before the thermodynamic equilibrium between the OH radical and water molecules can be reached. Therefore, the complex $[(H_2O)_{20}\cdot OH]^{IN}$ is less favorable than either $[(H_2O)_{20}\cdot OH]^{OUT,SIDE}$ or $[(H_2O)_{20}\cdot OH]^{OUT,TOP}$ in a real physical system. This prediction is consistent with conclusions drawn by molecular dynamics simulations.[7]

Another important piece of information is the distance where the interaction between the two moieties approaches asymptotic values. The graph show that this distance (R_{OO}) is about 5.0 Å for both structures, which is consistent with that of the $(H_2O)_{20}\cdot HO_2$ complexes reported in the literature.[6] The quantum chemical calculation results provide new insight into the initial stage by which the OH radical accommodates into a water droplet. Moreover, the distance for that the OH radical bonds most strongly on the surface of a water droplet is 2.9 Å, which is also consistent with the result of the full optimization.

The quantum chemical results suggest that the accommodation of the OH free radical to the water droplet surface is due to complexation effects. To put these results in the context for understanding what could happen to atmospheric OH radicals in the presence of clouds, one has to look at the competition of OH accommodating onto/into water droplets. These results may explain the overprediction of the OH concentration by the actinic flux calculation relative to the SICIMS experiments in the work of Mauldin at al.[5] since some OH radicals are bound to water droplets in clouds and not detected experimentally.

Despite the fact that the $(H_2O)_{20}$ cluster structure used in this study differs from the $(H_2O)_{20}\cdot HO_2$ complex reported in the literature[6] and that slightly different binding energies are obtained, the complexations are similar for both systems. This suggests that the interaction between the water droplets and free radicals have a common interaction. Of particular interest is the difference in the location of the radical within each structure. In the case of the global minimum structure for $(H_2O)_{20}\cdot OH$ complexes, the radical is caged internally, whereas in the global minimum structure for $(H_2O)_{20}\cdot HO_2$, the free radical is located outside of the water cluster; this contrast results from the electronic structure differences between OH and HO_2 radicals. This difference in radical location also implies that the most stable configuration of the complex formed between a water droplet and different free radicals may not be identical.

In order to study the impact of water cluster size on the interaction with the OH radical, the mTTM[22] model and TTM2-R empirical potential model[23–26] are used to optimize the structure of the $(H_2O)_{24}$ and $(H_2O)_{28}$ complexes and their corresponding OH complexes $[(H_2O)_{24}\cdot OH]$ and $[(H_2O)_{28}\cdot OH]$, as shown in Figures 10a−c and 11a−c. The initial guess of the spherical structures of the $(H_2O)_{24}$ and $(H_2O)_{28}$ complexes are from the studies in the literature.[48,49] In the optimization of these water cluster structures with the incorporation of a OH radical, two types of structures, for both the $[(H_2O)_{24}\cdot OH]$ and $[(H_2O)_{28}\cdot OH]$ complexes, are obtained. In one structure, the OH radical is bound outside of the water cluster, and the other the OH radical is accommodated inside of the cluster. The binding energies for $[(H_2O)_{24}\cdot OH]^{TOP}$ and $[(H_2O)_{24}\cdot OH]^{IN}$ are 9.3 and 10.5 kcal/mol, respectively, and for $[(H_2O)_{28}\cdot OH]^{TOP}$ and $[(H_2O)_{28}\cdot OH]^{IN}$, they are 10.15 and 11.28 kcal/mol, respectively. All of the structures are tested for their relaxation, and the calculations show that the binding energies for all of the $[(H_2O)_{24}\cdot OH]$ and $[(H_2O)_{28}\cdot OH]$ structures are from

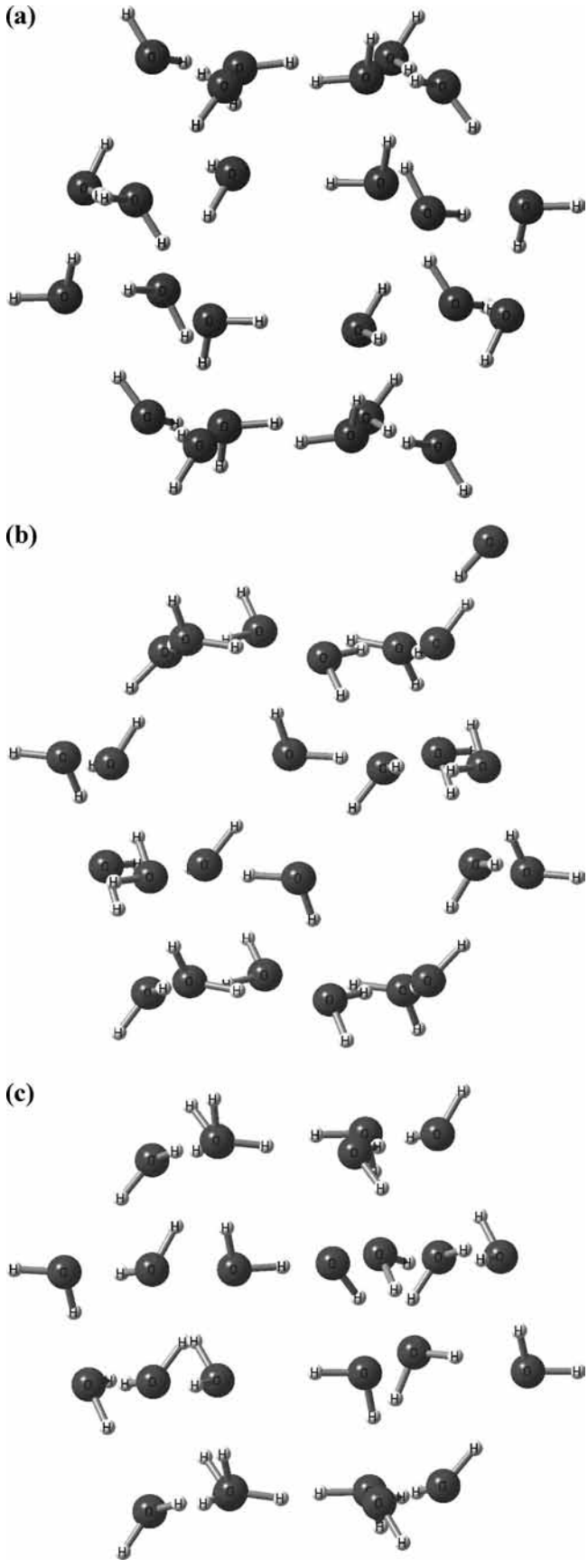

Figure 10. (a) The $(H_2O)_{24}$ structure. (b) The $[(H_2O)_{24}\cdot OH]^{TOP}$ structure. (c) The $[(H_2O)_{24}\cdot OH]^{IN}$ structure.

hydrogen bonding with the radical and not the relaxation of the water cluster. The results also show a trend consistent with the 20, 24, and 28 water cages in which the most stable complex is the one with the OH radical caged inside of the water cluster; this suggests that, regardless of the water cluster size, the OH radical prefers to be caged at 0 K.

We also constructed the contour of the potential energy surface by scanning the interacting energy at each distance of the oxygen atom in the OH radical to the closest oxygen atom in the water cluster. As shown in Figure 12, for the $[(H_2O)_{24}\cdot OH]$ and $[(H_2O)_{28}\cdot OH]$ complexes, the R_{OO} value for both structures is 2.8 Å, in good agreement with that of the $[(H_2O)_{20}\cdot OH]$ complexes, and the interacting radius of 5 Å corresponds well to the finding in the case of $[(H_2O)_{20}\cdot OH]$ too. The above findings suggest that the impact of the size of the water cluster $(H_2O)_n$ system on the binding of the OH radical should be insignificant when n is sufficiently large.

Since the relative thermodynamic stability of these isomers may change with variations in temperature and because chemical processes in the atmosphere usually occur at temperatures between 200 and 300 K, knowing the free energy behavior of each complex at different temperatures is essential. The free energies are therefore calculated from 100 to 500 K at the B3LYP/6-31G(d) level (Figure 13). The standard state at each temperature is defined as an isolated OH radical and $(H_2O)_{20}$ cluster. The free energies of all three complexes decrease with the increasing temperatures. At atmospheric temperatures of 200−300 K (Figure 13), the calculations show that the most stable configuration of the $[(H_2O)_{20}\cdot OH]$ complex in the atmosphere is $[(H_2O)_{20}\cdot OH]^{IN}$. This is consistent with the electronic structure result at 0 K. Although the anharmonicities are not considered, the relative magnitude of free energy for different complexes is qualitatively reliable, assuming that the contributions of anharmonicity for different complexes are comparable.

B. NBO Analysis. Weinhold et al.[21] developed a NBO theory, a wave function-orientated approach to analyze intermolecular interactions, which is used in this study to analyze the bonding feature of the $(H_2O)_{20}\cdot OH$ complexes. The purpose of this part of the study is to understand the nature of the interaction responsible for OH radical−water surface interaction. According to the NBO theory, each pair of valence natural hybrid obitals (NHOs) leads to a complementary pair of valence bonding and antibonding orbitals, and the treatment of bond−antibond interactions constitutes its most unique and characteristic contribution toward extending the Lewis structure concepts of valence theory.[17] A standard Rayleigh−Schrödinger perturbation treatment of the effect of mixing an occupied bond and an empty antibond leads to the estimated second-order energy lowering.[17] Since a hydrogen bond is formed by a lone pair and an antibond and can be directly reflected by the second-order interactions between occupied and virtual natural bond orbitals in NBO theory, a NBO analysis can give direct insight into the interactions that stabilize the hydrogen-bonding complexes.

For the purpose of finding out the difference in bonding features between a OH radical complexed with the water cluster and one with two water molecules in the same geometry, NBO calculation and analysis are performed. The isolated three-molecule structures are shown in Figures 4, 6, and 8.

The interaction energies between the lone pairs (n) on the O atoms and anti σ bonds (σ^*) of OH for the $[(H_2O)_{20}\cdot OH]^{OUT,SIDE}$ structure are shown in Table 2. In the $[(H_2O)_{20}\cdot OH]^{OUT,SIDE}$ complex, the two lone electron pairs of O_4 both participate in a hydrogen-bonding interaction with the σ^* bonds of OH. The orbital interaction between $n(O_4)$ and $\sigma^*(O_9-H_{37})$ is shown in

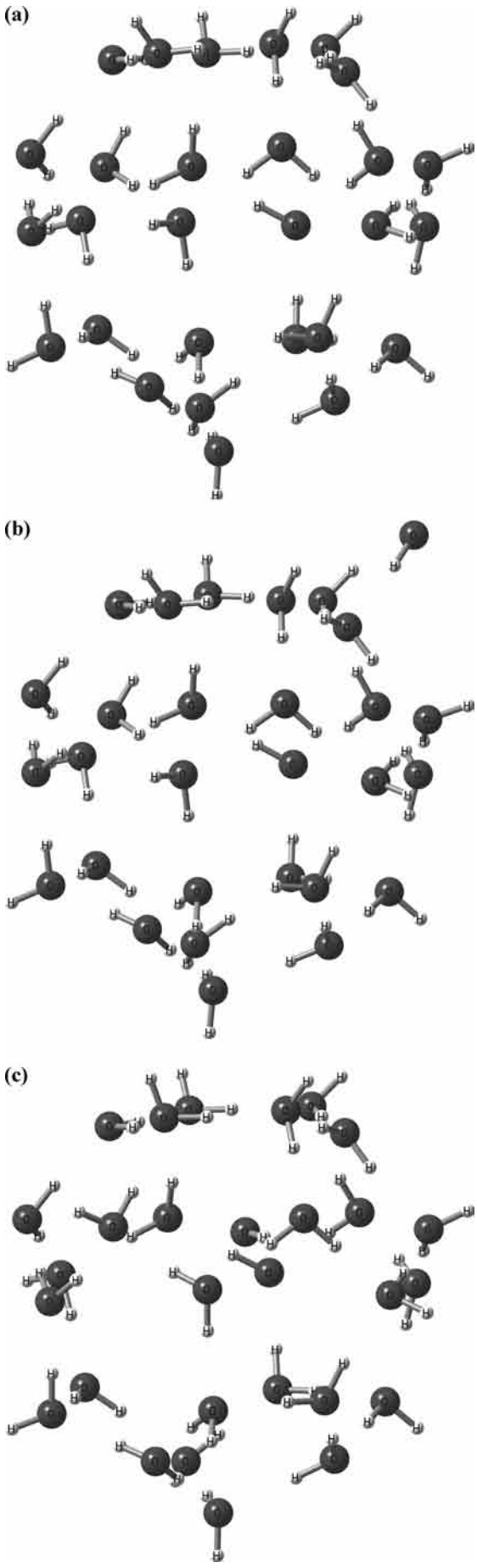

Figure 11. (a) The $(H_2O)_{28}$ structure. (b) The $[(H_2O)_{28}\bullet OH]^{TOP}$ structure. (c) The $[(H_2O)_{28}\bullet OH]^{IN}$ structure.

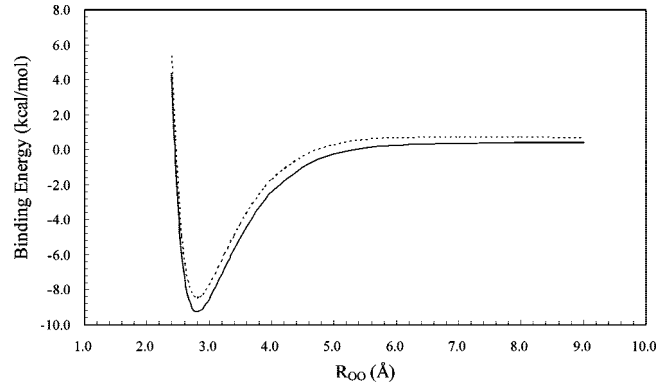

Figure 12. The potential energy curves of the OH radical to the $(H_2O)_{24}$ (solid line) and $(H_2O)_{28}$ (dash line) systems by the predicted mTTM potential.

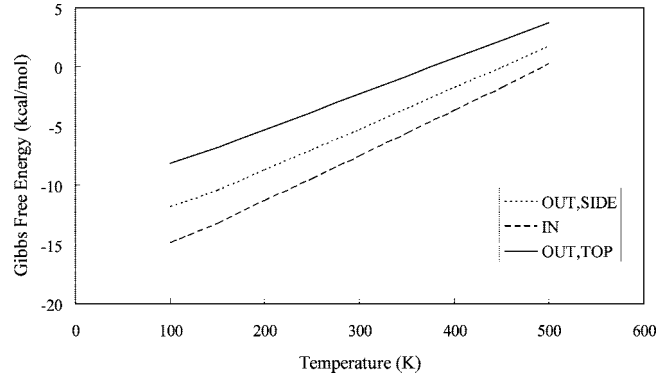

Figure 13. Free-energy curve of the complexes at the B3LYP/6-31G(d) level.

TABLE 2: NBO Data of the $[(H_2O)_{20}\cdot OH]^{OUT,SIDE}$ Structure at the Level of B3LYP/6-31G(d)[a]

	$OH\cdot(H_2O)_2$ (kcal/mol)			$OH\cdot(H_2O)_{20}$ (kcal/mol)		
	α	β	total	α	β	total
$n_1(O_4) \rightarrow \sigma^*(O_9-H_{37})$	0.20	0.19	0.39	2.36	2.30	4.66
$n_2(O_4) \rightarrow \sigma^*(O_9-H_{37})$	7.95	7.94	15.89	4.99	5.07	10.06
$n_1(O_9) \rightarrow \sigma^*(O_{61}-H_{62})$	0.30	0.31	0.61	2.97	3.67	6.64
$n_2(O_9) \rightarrow \sigma^*(O_{61}-H_{62})$	11.57	11.12	22.69	9.45	8.06	17.51
$n_2(O_{61}) \rightarrow \sigma^*(O_4-H_{28})$	0.37	0.33	0.70	0.38	0.38	0.76
$n_3(O_{61}) \rightarrow \sigma^*(O_4-H_{28})$	8.34	9.07	17.41	8.64	9.53	18.17

[a] Definitions: n = lone pair; σ^* = anti σ bond; 1, 2 and 3 denote different lone pairs.

Figure 14a and b . As seen in this figure, the overlapping of one $[n_1(O_4) \rightarrow \sigma^*(O_9-H_{37})]$ interaction is much less than that of the other $[n_2(O_4) \rightarrow \sigma^*(O_9-H_{37})]$, which is reflected by the interaction energy difference as listed in Table 2. A comparable trend is also found for the interaction between O_9 and $O_{61}-H_{62}$, as shown in Figure 14c and d . However, the relative magnitude of the contribution to the total interaction $[(n_1 \rightarrow \sigma^*) + (n_2 \rightarrow \sigma^*)]$ between the two lone pair $[(n_1 \rightarrow \sigma^*)$ and $(n_2 \rightarrow \sigma^*)]$ is quite different for the two complexes. In the case of $(H_2O)_2\cdot OH$, the $n_1 \rightarrow \sigma^*$ interaction between O_4 and O_9-H_{37} is only 0.39 kcal/mol (2.4% of the total interaction), while in $(H_2O)_{20}\cdot OH$, this interaction is found to be 4.7 kcal/mol (31.6% of the total interaction). Similarly, the $n_1 \rightarrow \sigma^*$ interaction between O_9 and $O_{61}-H_{62}$ is only 0.6 kcal/mol in $(H_2O)_2\cdot OH$ (2.6%) but is as high as 6.64 kcal/mol in $(H_2O)_{20}\cdot OH$ (27.5%). Despite these differences in the contribution, it is worth noting that the total interaction energies $[(n_1 \rightarrow \sigma^*) + (n_2 \rightarrow \sigma^*)]$ of $n(O_9) \rightarrow \sigma^*(O_{61}-H_{62})$ and $n(O_4) \rightarrow \sigma^*(O_9-H_{37})$ are nearly equivalent

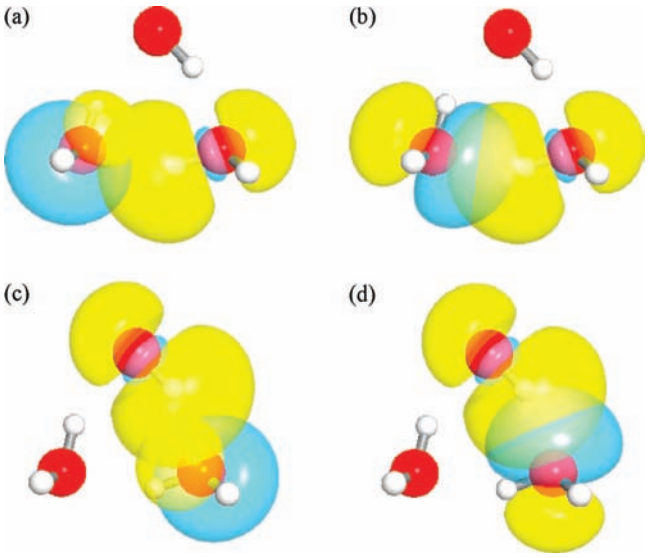

Figure 14. (a) The orbital interaction of $n_1(O_4) \rightarrow \sigma^*(O_9-H_{37})$ in the $[(H_2O)_{20}\cdot OH]^{OUT,SIDE}$ complex. (b) The orbital interaction of $n_2(O_4) \rightarrow \sigma^*(O_9-H_{37})$ in the $[(H_2O)_{20}\cdot OH]^{OUT,SIDE}$ complex. (c) The orbital interaction of $n_1(O_9) \rightarrow \sigma^*(O_{61}-H_{62})$ in the $[(H_2O)_{20}\cdot OH]^{OUT,SIDE}$ complex. (d) The orbital interaction of $n_2(O_9) \rightarrow \sigma^*(O_{61}-H_{62})$ in the $[(H_2O)_{20}\cdot OH]^{OUT,SIDE}$ complex.

when comparing $(H_2O)_{20}\cdot OH$ with $(H_2O)_2\cdot OH$, as listed in Table 2. The above findings indicate that the alignment of the 2p obital, lone electron pairs on the oxygen atoms in the water molecules are influenced by the surrounding water molecules interacting with the OH radical. This result can be explained as the stereoelectronic effect of other water molecules in the cluster on those interacting directly with the OH radical. Another interesting finding is that the $n(O_{61}) \rightarrow \sigma^*(O_4-H_{28})$ interaction is relatively the same for the two complexes. This means that the above effect probably occurs only in the water molecules of the cluster instead of in the OH radical. From the NBO analysis, it can be concluded that the interaction between ·OH and a water droplet surface is not simply a localized effect. When the binding energies between $(H_2O)_{20}\cdot OH$ and $(H_2O)_2\cdot OH$ are compared, the difference in binding energy is only 0.8 kcal/mol for $[(H_2O)_{20}\cdot OH]^{OUT,SIDE}$, suggesting that the complexation is a localized effect. However, the NBO analysis also suggests that the stereoelectronic effect is very significant for the interaction between a water cluster and a OH radical. This conclusion is different from that drawn from the interaction between HO_2 and water droplets,[16] in which it has been shown that the $HO_2-(H_2O)_{20}$ interaction is localized by NBO analysis. The present result suggests that different effects may occur among water molecules in the water droplets when interacting with different free radicals.

The data for the structure $[(H_2O)_{20}\cdot OH]^{OUT,TOP}$ are listed in Table 3, and the orbital overlapping graphs are shown in Figure 15a and b. The interaction energy of the two lone pairs on O_{19} (n_1 and n_2) with $\sigma^*(O_{20}-H_{59})$ and $\sigma^*(O_{61}-H_{62})$ both differ between the $(H_2O)_2\cdot OH$ and $(H_2O)_{20}\cdot OH$ complexes (Table 3). This difference probably also results from similar effect as in the case of $[(H_2O)_{20}\cdot OH]^{OUT,SIDE}$. The difference between $[(H_2O)_{20}\cdot OH]^{OUT,SIDE}$ and $[(H_2O)_{20}\cdot OH]^{OUT,TOP}$ is in their changes in the total interaction energies. The total interaction energies of $n(O_{19}) \rightarrow \sigma^*(O_{20}-H_{59})$ and $n(O_{19}) \rightarrow \sigma^*(O_{61}-H_{62})$ in $[(H_2O)_{20}\cdot OH]^{OUT,TOP}$ increase by 6.1 and 3.3 kcal/mol, respectively. These increments indicate that the stereoelectronic effect may result in a significant change in the interaction energy between the OH radical and the water droplet surface. The

TABLE 3: NBO Data of $[(H_2O)_{20}\cdot OH]^{OUT,TOP}$ Structure at the Level of B3LYP/6-31G(d)

	$OH\cdot(H_2O)_2$ (kcal/mol)			$OH\cdot(H_2O)_{20}$ (kcal/mol)		
	α	β	total	α	β	total
$n_1(O_{19}) \rightarrow \sigma^*(O_{20}-H_{59})$	1.31	0.99	2.30	0.55	0.34	0.89
$n_2(O_{19}) \rightarrow \sigma^*(O_{20}-H_{59})$	7.79	8.11	15.9	11.09	11.40	22.49
$n_1(O_{19}) \rightarrow \sigma^*(O_{61}-H_{62})$	3.88	4.12	8.00	6.41	6.54	12.95
$n_2(O_{19}) \rightarrow \sigma^*(O_{61}-H_{62})$	4.77	4.31	9.08	3.96	3.47	7.43
$n_1(O_{61}) \rightarrow \sigma^*(O_{20}-H_{60})$	0.21	0.21	0.42	0.25	0.25	0.50
$n_2(O_{61}) \rightarrow \sigma^*(O_{20}-H_{60})$	5.25	5.79	11.04	5.80	6.40	12.20

n = lone pair, σ^*= anti σ bond, 1 and 2 denote different lone pairs

interaction of $n(O_{61}) \rightarrow \sigma^*(O_{20}-H_{60})$ does not change from $(H_2O)_2\cdot OH$ to $(H_2O)_{20}\cdot OH$ as it does in $[(H_2O)_{20}\cdot OH]^{OUT,SIDE}$; therefore, the same conclusion that the orbital orientation changes occur on the water molecules instead of the OH radical can be drawn. These consistencies in delocalization between the structures $[(H_2O)_{20}\cdot OH]^{OUT,SIDE}$ and $[(H_2O)_{20}\cdot OH]^{OUT,TOP}$ strongly suggest that the stereoelectronic effect among water molecules, when a OH radical complexes to the surface of a water droplet, cannot be ignored.

The NBO data for the global minimum $[(H_2O)_{20}\cdot OH]^{IN}$ are listed in Table 4. Only the strongest interaction of $n(O_{15}) \rightarrow \sigma^*(O_{61}-H_{62})$ and $n(O_{61}) \rightarrow \sigma^*(O_{12}-H_{43})$ is shown. The interaction energies for $(H_2O)_2\cdot OH$ and $(H_2O)_{20}\cdot OH$ for $[(H_2O)_{20}\cdot OH]^{IN}$ are very similar, as seen in Table 4, which is different from the other two structures. This implies that the three-molecule interaction is dominated by a localized effect. Since these interactions constitute the main components of stabilization energy, the dominant effect for the OH radical cage by waters is a result of a localization interaction. It is also found that there are also some other small long-range interactions such as $n(O_9) \rightarrow \sigma^*(O_{61}-H_{62})$, $n(O_{10}) \rightarrow \sigma^*(O_{61}-H_{62})$, $n(O_{14}) \rightarrow \sigma^*(O_{61}-H_{62})$, $n(O_{61}) \rightarrow \sigma^*(O_{14}-H_{47})$, $n(O_{61}) \rightarrow \sigma^*(O_6-H_{31})$, $n(O_{61}) \rightarrow \sigma^*(O_4-H_{27})$, and $n(O_{61}) \rightarrow \sigma^*(O_5-H_{29})$, from which the structure can gain some extra stability.

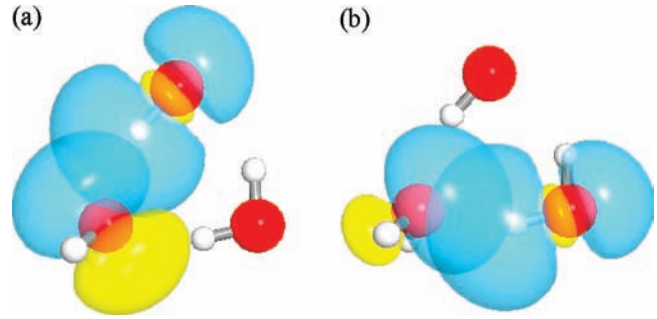

Figure 15. (a) The orbital interaction of $n_1(O_{19}) \rightarrow \sigma^*(O_{61}-H_{62})$ in the $[(H_2O)_{20}\cdot OH]^{OUT,SIDE}$ complex. (b) The orbital interaction of $n_2(O_{19}) \rightarrow \sigma^*(O_{20}-H_{59})$ in the $[(H_2O)_{20}\cdot OH]^{OUT,SIDE}$ complex.

TABLE 4: NBO Data of $[(H_2O)_{20}\cdot OH]^{IN}$ Structure at the Level of B3LYP/6-31G(d)[a]

	$OH\cdot(H_2O)_2$ (kcal/mol)			$OH\cdot(H_2O)_{20}$ (kcal/mol)		
	α	β	total	α	β	total
$n_1(O_{15}) \rightarrow \sigma^*(O_{61}-H_{62})$	0.43	0.39	0.82	0.42	0.79	1.21
$n_2(O_{15}) \rightarrow \sigma^*(O_{61}-H_{62})$	14.80	14.22	29.02	14.41	13.33	27.74
$n_1(O_{61}) \rightarrow \sigma^*(O_{12}-H_{43})$	0.21	0.26	0.47	0.44	0.45	0.89
$n_2(O_{61}) \rightarrow \sigma^*(O_{12}-H_{43})$	7.40	8.08	15.48	8.14	8.81	16.95

[a] Definitions: n = lone pair; σ^*= anti σ bond; 1 and 2 denote different lone pairs.

IV. Conclusions

In this work, results from a theoretical study on the interaction between the •OH radical and the $(H_2O)_{20}$, $(H_2O)_{24}$, and $(H_2O)_{28}$ clusters, as simple models of a water cluster on an aerosol surface, show that there may be three different types of hydrogen-bond complexes for the $(H_2O)_{20}$ case and two different types of hydrogen-bond complexes for $(H_2O)_{24}$ and $(H_2O)_{28}$. From the energies of the three complexes of $(H_2O)_{20}$•OH, based on quantum chemical calculations, we find that the structure with •OH caged inside of a water droplet is most stable at 0 K. This internal cage structure is further confirmed to be the thermodynamically most stable structure at atmospheric temperatures by free-energy calculations. Potential energy surface scans of the $(H_2O)_{20}$•OH give insight into how the radical approaches a cloud droplet. The distance when the noticeable radical−water interaction starts is found to be 5.0 Å. These results are compared with those of the OH complexes binding to larger water clusters by using the recently developed empirical potential, and similar conclusions are drawn. With the similarities of the structure and energy among the three types of $(H_2O)_n$•OH ($n = 20, 24, 28$) complexes, the size impact of the water clusters on the binding of the OH radical is found to be insignificant. Another important finding is that the interaction between OH and a water surface in the atmosphere is not localized. The NBO analysis results show that the stereoelectronic effect on water molecules may result in alterations of the interaction energy with a OH radical when the OH radical binds onto the surface of a water droplet. In clouds, since there is a high concentration of water molecules, the present study suggests that an abundance of available OH radical will decrease through the complexation of OH radicals with water droplets and transportation with the aerosols. On the basis of the previous works[50–53] and the calculation results presented here, we can picture the accommodation process of the OH radical on the aerosols in the atmosphere. Aerosols formed by their core and surface water molecules during the movement in the atmosphere act as open surface sites for the free radicals. The free radicals such as the OH radical can bind to the surface of the aerosol via hydrogen bonding at the aerosol−air interface and are consequently transported with the aerosols in the atmosphere. These findings have important implications for the processing of organic materials by atmospheric aerosols.

Acknowledgment. This research was performed, in part, by using the Molecular Science Computing Facility (MSCF) in the William R. Wiley Environmental Molecular Sciences Laboratory at the Pacific Northwest National Laboratory. The MSCF is funded by the Office of Biological and Environmental Research in the U.S. Department of Energy. Battelle operates Pacific Northwest National Laboratory for the DOE. We also appreciate Professor Tsun-Mei Chang from the Department of Chemistry, University of Wisconsin, Parkside, for her warmhearted help in providing numerous constructive suggestions for improving this paper.

Supporting Information Available: Supporting tables. This material is available free of charge via the Internet at http://pubs.acs.org.

References and Notes

(1) Seinfeld, J. H.; Pandis, S. N. *Atmospheric Chemistry and Physics*; John Wiley & Sons Inc: New York, 1998.

(2) Wayne, R. P. *Chemistry of Atmospheres*; Oxford University: Oxford, U.K., 2000.

(3) McKeen, S. A.; Mount, G.; Eisele, F.; Williams, E.; Harder, J.; Goldan, P.; Kuster, W.; Liu, S. C.; Baumann, K.; Tanner, D.; Fried, A.; Sewell, S.; Cantrell, C.; Shetter, R. *J. Geophys. Res.* **2002**, *102*, 6467.

(4) Liu, S. C.; Trainer, M.; Carroll, M. A.; Hubler, G.; Montzka, D. D.; Norton, R. B.; Ridley, B. A.; Walega, J. G.; Atlas, E. L.; Heikes, B. G.; Heubert, B. J.; Warren, W. *J. Geophys. Res.* **1992**, *97*, 10463.

(5) Mauldin, R. L., III; Madronich, S.; Flocke, S. J.; Eisele, F. L.; Frost, G. J.; Prevot, A. S. H. *Geophys. Res. Lett.* **1997**, *24*, 3033.

(6) Shi, Q.; Belair, S. D.; Francisco, J. S.; Kais, S. *Proc. Natl. Acad. Sci. U.S.A.* **2003**, *100*, 9686.

(7) Roeselova, M.; Jungwirth, P.; Tobias, D. J.; Gerber, R. B. *J. Phys. Chem. B* **2003**, *107*, 12690.

(8) Roeselova, M.; Vieceli, J.; Dang, L. X.; Garrett, B. C.; Tobias, D. J. *J. Am. Chem. Soc.* **2004**, *126*, 16308.

(9) Cabral do Couto, P.; Guedes, R. C.; Costa Carbral, B. J. *J. Chem. Phys.* **2003**, *119*, 7344.

(10) Shin, J. W.; Hammer, N. I.; Diken, E. G.; Johnson, M. A.; Walters, R. S.; Jaeger, T. D.; Duncan, M. A.; Christie, R. A.; Jordan, K. D. *Science* **2004**, *304*, 1137.

(11) Miyazaki, M.; Fujii, A.; Ebata, T.; Mikami, N. *Science* **2004**, *304*, 1134.

(12) Coe, J. V.; Earhart, A. D.; Cohen, M. H.; Hoffman, G. J.; Sarkas, H. W.; Bowen, K. H. *J. Chem. Phys.* **1997**, *107*, 6023.

(13) Tobias, D. J.; Jungwirth, P.; Parrinello, M. *J. Chem. Phys.* **2001**, *114*, 7036.

(14) Perera, L.; Berkowitz, M. L. *J. Chem. Phys.* **1993**, *100*, 3085.

(15) Gilligan, J. J.; Castleman, A. W., Jr *J. Phys. Chem. A* **2001**, *105*, 5601.

(16) Belair, S. D.; Hernandez, H.; Francisco, J. S. *J. Am. Chem. Soc.* **2004**, *126*, 3024.

(17) Weinhold, F. Natural Bond Orbital Methods, In *Encyclopedia of Computational Chemistry*; Schleyer, P. v. R., Allinger, N. L., Clark, T., Gasteiger, J., Kollman, P. A., Schaefer, H. F., III, Schreiner, P. R., Eds.; John Wiley & Sons: New York, 1998; Vol. 3, p 1792.

(18) Reed, A. E.; Curtiss, L. A.; Weinhold, F. *Chem. Rev.* **1988**, *88*, 899.

(19) Weinhold F.; Carpenter, J. E. In *The Structure of Small Molecules and Ions*; Naaman, R., Vager, Z., Eds.; Plenum: New York, 1988; p 227.

(20) Weinhold, F. In *Computational Methods in Organic Photochemistry: Molecular and Supramolecular Photochemistry*; Kutateladze, A. G., Ed.; Taylor & Francis/CRC Press: Boca Raton FL, 2005; p 393.

(21) Froster, J. P.; Weinhold, F. *J. Am. Chem. Soc.* **1980**, *102*, 7211.

(22) Du, S.; Francisco, J. S.; Schenter, G. K.; Iordanov, T. D.; Garrett, B. C.; Dupuis, M.; Li, J. *J. Chem. Phys.* **2006**, *124*, 224318.

(23) Burnham, C. J.; Li, J. C.; Xantheas, S. S.; Leslie, M. *J. Chem. Phys.* **1999**, *110*, 4566.

(24) Burnham, C. J.; Xantheas, S. S. *J. Chem. Phys.* **2002**, *116*, 1479.

(25) Xantheas, S. S.; Burnham, C. J.; Harrison, R. J. *J. Chem. Phys.* **2002**, *116*, 1493.

(26) Burnham, C. J.; Xantheas, S. S. *J. Chem. Phys.* **2002**, *116*, 1500.

(27) Cioslowski, J.; Nanayakkara, A. *Int. J. Mod. Phys. B* **1992**, *6*, 3687.

(28) Maheshwary, S.; Patel, N.; Sathyamurthy, N.; Kulkarni, A. D.; Gadre, S. R. *J. Phys. Chem. A.* **2001**, *105*, 10525.

(29) Lee, C.; Chen, H.; Fitzgerald, G. *J. Chem. Phys.* **1995**, *102*, 1266.

(30) Wales, D. J.; Hodges, M. P. *Chem. Phys. Lett.* **1998**, *286*, 65.

(31) Schaefer, H. F. *Quantum Chemistry*; Clarendon: Oxford, 1984.

(32) Becke, A. D. *J. Chem. Phys.* **1993**, *98*, 5648.

(33) Frisch, M. J.; Head-Gordon, M.; Pople, J. A. *Chem. Phys. Lett.* **1990**, *166*, 281.

(34) Head-Gordon, M.; Head-Gordon, T. *Chem. Phys. Lett.* **1994**, *220*, 122.

(35) Moeller, C.; Plesset, M. S. *Phys. Rev.* **1934**, *46*, 618.

(36) Frisch, M. J. Trucks, G. W.; Schlegel, H. B.; Scuseria, G. E.; Robb, M. A.; Cheeseman, J. R.; Montgomery, J. A.; Jr Vreven, T.; Kudin, K. N.; Burant, J. C.; Millam, J. M.; Iyengar, S. S.; Tomasi, J.; Barone, V.; Mennucci, B.; Cossi, M.; Scalmani, G.; Rega, N.; Petersson, G. A.; Nakatsuji, H.; Hada, M.; Ehara, M.; Toyota, K.; Fukuda, R.; Hasegawa, J.; Ishida, M.; Nakajima, T.; Honda, Y.; Kitao, O.; Nakai, H.; Klene, M.; Li, X.; Knox, J. E.; Hratchian, H. P.; Cross, J. B.; Bakken, V.; Adamo, C.; Jaramillo, J.; Gomperts, R.; Stratmann, R. E.; Yazyev, O.; Austin, A. J.; Cammi, R.; Pomelli, C.; Ochterski, J. W.; Ayala, P. Y.; Morokuma, K.; Voth, G. A.; Salvador, P.; Dannenberg, J. J.; Zakrzewski, V. G.; Dapprich, S.; Daniels, A. D.; Strain, M. C.; Farkas, O.; Malick, D. K.; Rabuck, A. D.; Raghavachari, K.; Foresman, J. B.; Ortiz, J. V.; Cui, Q.; Baboul, A. G.; Clifford, S.; Cioslowski, J.; Stefanov, B. B.; Liu, G.; Liashenko, A.; Piskorz, P.; Komaromi, I.; Martin, R. L.; Fox, D. J.; Keith, T.; Al-Laham, M. A.; Peng, C. Y.; Nanayakkara, A.; Challacombe, M.; Gill, P. M. W.; Johnson, B.; Chen, W.; Wong, M. W.; Gonzalez, C.; Pople, J. A. *Gaussian 98*, revision A.9; Gaussian, Inc.: Pittsburgh, PA, 1998.

(37) Frisch, M. J. Trucks, G. W.; Schlegel, H. B.; Scuseria, G. E.; Robb, M. A.; Cheeseman, J. R.; Montgomery, J. A.; Jr Vreven, T.; Kudin, K. N.; Burant, J. C.; Millam, J. M.; Iyengar, S. S.; Tomasi, J.; Barone, V.; Mennucci, B.; Cossi, M.; Scalmani, G.; Rega, N.; Petersson, G. A.;

Nakatsuji, H.; Hada, M.; Ehara, M.; Toyota, K.; Fukuda, R.; Hasegawa, J.; Ishida, M.; Nakajima, T.; Honda, Y.; Kitao, O.; Nakai, H.; Klene, M.; Li, X.; Knox, J. E.; Hratchian, H. P.; Cross, J. B.; Bakken, V.; Adamo, C.; Jaramillo, J.; Gomperts, R.; Stratmann, R. E.; Yazyev, O.; Austin, A. J.; Cammi, R.; Pomelli, C.; Ochterski, J. W.; Ayala, P. Y.; Morokuma, K.; Voth, G. A.; Salvador, P.; Dannenberg, J. J.; Zakrzewski, V. G.; Dapprich, S.; Daniels, A. D.; Strain, M. C.; Farkas, O.; Malick, D. K.; Rabuck, A. D.; Raghavachari, K.; Foresman, J. B.; Ortiz, J. V.; Cui, Q.; Baboul, A. G.; Clifford, S.; Cioslowski, J.; Stefanov, B. B.; Liu, G.; Liashenko, A.; Piskorz, P.; Komaromi, I.; Martin, R. L.; Fox, D. J.; Keith, T.; Al-Laham, M. A.; Peng, C. Y.; Nanayakkara, A.; Challacombe, M.; Gill, P. M. W.; Johnson, B.; Chen, W.; Wong, M. W.; Gonzalez, C.; Pople, J. A. *Gaussian 03*, revision B.05; Gaussian, Inc.: Pittsburgh, PA, 2003.

(38) Kendall, R. A.; Apra, E.; Bernholdt, D. E.; Bylaska, E. J.; Dupuis, M.; Fann, G. I.; Harrison, R. J.; Ju, J.; Nichols, J. A.; Nieplocha, J.; Straatsma, T. P.; Windus, T. L.; Wong, A. T. *Comput. Phys. Commun.* **2000**, *128*, 260.

(39) See http://www.emsl.pnl.gov for more information.

(40) Glendening, E. D.; Badenhoop, J. K.; Reed, A. E.; Carpenter, J. E.; Bohnmann, J. A.; Morales, C. M.; Weinhold, F. *NBO 5.0*; Theoretical Chemistry Institute, University of Wisconsin: Madison, WI, 2001.

(41) Boys, S. F.; Bernardi, F. *Mol. Phys.* **1970**, *19*, 553.

(42) Hampel, H.-J.; Werner, J. *Chem. Phys.* **1996**, *104*, 6286.

(43) Raghavachari, K.; Trucks, G. W.; Pople, J. A.; Head-Gordon, M. *Chem. Phys. Lett.* **1989**, *157*, 479.

(44) Scuseria, G. E. *Chem. Phys. Lett.* **1991**, *176*, 27.

(45) Knowles, P. J.; Hampel, C.; Werner, H. *J. Chem. Phys.* **1993**, *99*, 5219.

(46) Kendall, R. A.; Dunning, T. H., Jr.; Harrison, R. J. *J. Chem. Phys.* **1992**, *96*, 6796.

(47) Woon, D. E.; Dunning, T. H., Jr *J. Chem. Phys.* **1993**, *98*, 1358.

(48) Herbert, J. M.; Head-Gordon, M. *Phys. Chem. Chem. Phys.* **2006**, *8*, 68.

(49) Khan, A. *THEOCHEM* **2003**, *664*, 237.

(50) Hanson, D. R.; Ravishankara, A. R.; Solomon, S. *J. Geophys. Res.* **1994**, *99*, 3615.

(51) Gertner, B. J.; Hynes, J. T. *Science* **1996**, *271*, 1563.

(52) Mauldin, R. L., III; Frost, G. J.; Chen, G.; Tanner, D. J.; Prevot, A. S. H.; Davis, D. D.; Eisele, F. L. *J. Geophys. Res.* **1998**, *103*, 16713.

(53) Saylor, R. D. *Atmos. Environ.* **1997**, *31*, 3653.

JP710509H